Dynamics and control of a multimode laser: Reduction of space-dependent rate equations to a low-dimensional system

K. Pyragas,[1,2,*] F. Lange,[1] T. Letz,[1] J. Parisi,[1] and A. Kittel[1]
[1]*Department of Energy and Semiconductor Research, Faculty of Physics, University of Oldenburg, D-26111 Oldenburg, Germany*
[2]*Semiconductor Physics Institute, LT-2600 Vilnius, Lithuania*
(Received 30 June 2000; published 18 December 2000)

We suggest a quantitatively correct procedure for reducing the spatial degrees of freedom of the space-dependent rate equations of a multimode laser that describe the dynamics of the population inversion of the active medium and the mode intensities of the standing waves in the laser cavity. The key idea of that reduction is to take advantage of the small value of the parameter that defines the ratio between the population inversion decay rate and the cavity decay rate. We generalize the reduction procedure for the case of an intracavity frequency doubled laser. Frequency conversion performed by an optically nonlinear crystal placed inside the laser cavity may cause a pronounced instability in the laser performance, leading to chaotic oscillations of the output intensity. Based on the reduced equations, we analyze the dynamical properties of the system as well as the problem of stabilizing the steady state. The numerical analysis is performed considering the specific system of a Nd:YAG (neodymium-doped yttrium aluminum garnet) laser with an intracavity KTP (potassium titanyl phosphate) crystal.

DOI: 10.1103/PhysRevE.63.016204 PACS number(s): 05.45.−a

I. INTRODUCTION

Intensive investigations of fundamental nonlinear dynamic phenomena in a solid-state laser with intracavity frequency doubling began with an observation of Baer [1], who reported large intensity pulsations in a multimode laser system. The latter consisted of a diode-pumped Nd:YAG (yttrium aluminum garnet) laser and an optically nonlinear KTP (potassium titanyl phosphate)) crystal placed inside the laser cavity. The KTP crystal is used to convert infrared (1064 nm) Nd:YAG laser radiation into visible green light (532 nm) by the process of second harmonic and sum frequency generation. In order to explain the dynamic instability observed in experiment, Baer proposed a phenomenological set of coupled rate equations for the mode intensities and gains. Mandel and Wu [2] subsequently carried out the stability analysis for Baer's equations. A significant advance in the ''green problem'' was made by Oka and Kubota [3], who recognized that the polarization of the cavity modes plays a critical role in the laser dynamics and, therefore, used an intracavity quarter-wave plate to stabilize the laser output. Their theoretical analysis, however, was limited to a model that includes only two orthogonally polarized cavity modes. The most impressive success with Baer's model was achieved by James, Harrel, Bracikowski, Wiesenfeld, and Roy (JHBWR) [4–6], who adapted the model to include birefringence of the active medium and the doubling crystal and demonstrated its behavior in an extensive set of dynamic regimes, including chaos, intermittency, and antiphase dynamics. Liu *et al.* [7] recently developed a more general model of the laser system that includes both the amplitudes and the phases of the electric fields of the infrared light.

In our previous work [8], we proposed that unstable steady states of the multimode laser system can be stabilized by modulating the laser pump rate with a feedback signal composed of two experimentally available quantities, namely, the total intensities of the infrared light polarized in two different orthogonal directions. Using the JHBWR model, we have obtained promising prospects for experimental implementation. As a result of the analysis it follows that stability of the steady state can be achieved for an arbitrarily large number of modes and can be maintained for an arbitrarily large pump rate. In a real-world experiment, however, we [9] as well as Schenck and Dressler [10] were able to stabilize the steady state only for a pump rate not too much above the laser threshold and only for the case of a few oscillating modes. Such incompatibility of theoretical and experimental results is probably related to a certain coarseness of the JHBWR model. The problem of stabilizing the laser output requires a more sophisticated model. In particular, the model should accurately describe the system dynamics close to the steady states.

The JHBWR model as well as other similar models of multimode solid-state lasers are derived from the space-dependent coupled rate equations of Tang, Statz, and deMars (TSM) [11] that describe the population inversion and mode intensities of the standing waves in the laser cavity. Due to the complicated spatial distribution of the population inversion, the TSM model is difficult to analyze both analytically and numerically. Therefore, various approximations are used, in order to simplify the model. The most popular approach is to expand the population inversion into Fourier series and truncate it at the first harmonics of the lasing modes [11]. Another scheme of reducing the spatial degrees of freedom is used in Ref. [6], where an infinite set of ordinary differential equations is also truncated artificially. Thus, both reduction procedures can be justified only qualitatively. Moreover, the approximations used in the JHBWR model lead to phenomenological parameters that are difficult to estimate theoretically, e.g., the cross-saturation parameters.

In this paper, we derive a reduced system of ordinary

*Electronic address: pyragas@kes0.pfi.lt

differential equations whose solutions are in good quantitative agreement with those of the original TSM space-dependent rate equations. In our reduction procedure, we take advantage of a small parameter that defines the ratio between the population inversion decay rate and the cavity decay rate. Depending on the structure of the laser system, we are able to estimate all parameters of our reduced model from theory. Like Viktorov, Klemer, and Karim [12], we take into account the fact that the laser cavity is not entirely filled with the active medium. On the basis of our actual model we reconsider the problem of stabilizing the steady state of the system originally looked at in our previous work [8].

The rest of the paper is organized as follows. The next section contains the description of the TSM model, the characteristic values of the parameters used in the numerical analysis, and the model equations in dimensionless form. In Sec. III, we describe the procedure of reducing the TSM space-dependent rate equations (without the KTP crystal) to a finite set of ordinary differential equations. We start from the case of a single-mode laser and then generalize our approach to a multimode case. We estimate the steady state solution of our model close to the laser threshold and analyze the transient dynamics of the system. In Sec. IV, the reduction procedure is generalized for the case of an intracavity frequency doubled laser. We introduce the terms responsible for the nonlinear frequency conversion due to the KTP crystal placed inside the laser cavity and show that this can lead to a chaotic instability in the laser performance. Section V is devoted to the problem of stabilizing the unstable steady state. We consider a proportional feedback technique where the pump rate of the laser is modulated by the output signal, composed of two total intensities of the infrared light polarized in two different orthogonal directions. In the appropriate parameter space, we numerically obtain the domains of stable laser performance. The results are summarized in the conclusions that are presented in Sec. VI.

II. SPACE-DEPENDENT RATE EQUATIONS

We begin with the well-known TSM coupled equations for the population inversion and mode intensities of the standing waves of a multimode laser, given in an early paper [11]:

$$\frac{d}{dt}\tilde{n}(z,t)=-\frac{\tilde{n}(z,t)-\tilde{n}_0}{\tau_f}-\sum_i D\tilde{g}_i\tilde{I}_i\left[1-\cos\frac{2m_i\pi}{L}z\right]\tilde{n}(z,t), \tag{1a}$$

$$\frac{d\tilde{I}_j}{dt}=-\frac{\alpha\tilde{I}_j}{\tau_c}+D\tilde{g}_j\tilde{I}_j\int_0^L\tilde{n}(z,t)\left[1-\cos\frac{2m_j\pi}{L}z\right]dz. \tag{1b}$$

Here, $\tilde{n}(z,t)$ is the spatially varying population inversion between the upper and lower lasing levels, $\tilde{n}_0$ the steady state value of $\tilde{n}(z)$ in the absence of stimulated emission, and τ_f the upper level fluorescence decay time. $D\tilde{g}_i$ denotes a stimulated emission coefficient appropriate for the ith mode and m_i the number of half wavelengths along the laser cavity. $\tilde{I}_i$ is the intensity of the ith mode and α the cavity loss parameter, which we take the same for all modes. $\tau_c=2L/c$ is the cavity round-trip time, where L is the optical length of the cavity and c the speed of light.

System (1) is usually considered for the case of homogeneous pumping, when $\tilde{n}_0$ is independent of the space variable z. Here, we take into account the effects of nonhomogeneous pumping. We consider the usual experimental situation when the YAG crystal is end-pumped by a phased array laser diode from the outside of the laser cavity. The pumping beam penetrates the YAG crystal up to the characteristic length k^{-1}, where k is the absorption coefficient of the YAG. In order to model nonhomogeneous pumping, we suppose that $\tilde{n}_0$ decays exponentially, $\tilde{n}_0=p_0\exp(-kz)$. Substituting this expression into Eqs. (1) and using the ansatz $\tilde{n}(z,t)=\exp(-kz)p(z,t)$, we obtain the equations

$$\frac{d}{dt}p(z,t)=-\frac{p(z,t)-p_0}{\tau_f}-\sum_i D\tilde{g}_i\tilde{I}_i\left[1-\cos\frac{2m_i\pi}{L}z\right]p(z,t), \tag{2a}$$

$$\frac{d\tilde{I}_j}{dt}=-\frac{\alpha\tilde{I}_j}{\tau_c}+D\tilde{g}_j\tilde{I}_j\int_0^L p(z,t)e^{-kz}\times\left[1-\cos\frac{2m_j\pi}{L}z\right]dz, \tag{2b}$$

similar to Eqs. (1) with the only difference that the integrand in Eq. (2b) is multiplied by an exponentially decaying factor. In the following, we suppose that $kL\gg1$ and replace the upper limit of the above integral by infinity. In a dimensionless form, these equations can be written as follows:

$$\frac{1}{\eta}\frac{d}{d\vartheta}n(x,\vartheta)=w-n(x,\vartheta)-n(x,\vartheta)\sum_i I_iu_i(x), \tag{3a}$$

$$\eta\frac{dI_j}{d\vartheta}=[-1+\langle n(x,\vartheta)u_j(x)\rangle]I_j. \tag{3b}$$

The new variables and parameters are

$$x=z/L,\quad \vartheta=t/T,\quad T=\sqrt{\tau_c\tau_f/\alpha},\quad \eta=\sqrt{\tau_c/\tau_f\alpha},$$

$$w=p_0\tau_cD\tilde{g}_0/\alpha k,\quad n=p\tau_cD\tilde{g}_0/\alpha k,\quad \text{and}\quad I_i=\tilde{I}_i\tau_fD\tilde{g}_0.$$

Here, $D\tilde{g}_0$ is the gain of the first lasing mode, which we label by the subscript $i=0$. We describe the normalized gains of the other modes with the Lorentzian

$$g_i\equiv\tilde{g}_i/\tilde{g}_0=(1+\xi i^2)^{-1},\quad \xi=(c/L\Delta\nu)^2, \tag{4}$$

where $\Delta\nu$ is the full width at half maximum of the YAG gain curve. The function $u_i(x)$ in Eqs. (3) is defined as

$$u_i(x)=g_i[1-\cos 2\pi(M+i)x], \tag{5}$$

TABLE I. Model parameters.

L (cm)	k (cm^{-1})	τ_f (μs)	$\Delta\nu$ (GHz)	α	ϵ	g
2.5	5	240	120	0.01	2×10^{-5}	0.1

where $M\gg1$ is the number of half wavelengths along the laser cavity for the first lasing mode. For the ith mode, the number of half wavelengths is $m_i=M+i$, $i=0,\pm1,\pm2,\ldots$. The angular brackets in Eq. (3b) denote the integral

$$\langle f(x)\rangle\equiv\kappa\int_0^\infty e^{-\kappa x}f(x)dx, \tag{6}$$

where $\kappa=kL$.

The characteristic model parameters that we utilize below for our numerical simulations are listed in Table I. From this collection of parameters, it follows that the cavity round-trip time τ_c is approximately 0.167 ns and the characteristic time scale of the intensity oscillations $T\approx2$ μs. The dimensionless parameters ξ and κ in Eq. (4) and Eq. (6) are $\xi\approx0.01$ and $\kappa\approx12.5$. The cavity accommodates $M\approx5\times10^4$ half wavelengths of the first lasing mode. The pump parameter w in Eq. (3a) is the main control parameter; it is scaled so that the first laser threshold occurs at $w=1$. The dimensionless parameter η defining the square root of the ratio between the inversion decay rate and the cavity decay rate is approximately 6.96×10^{-3}. In the next section, we use the smallness of this parameter to reduce the space-dependent Eqs. (3) to a finite set of ordinary differential equations.

III. REDUCTION OF THE LASER EQUATIONS

A. Single-mode laser

For a single-mode laser, $n(x,\vartheta)$ is a spatially periodic function, whose period l is equal to a half period of the first lasing mode, $l=1/M$. Thus, it is convenient to introduce a new space variable $s=x/l=xM$ normalized to this period and consider the space dependence in only one characteristic half-wavelength interval $s\in[0,1]$. Omitting, for simplicity, the subscript $i=0$ on the variables I_0 and u_0, we obtain the equations

$$\frac{1}{\eta}\frac{d}{d\vartheta}n(s,\vartheta)=w-n(s,\vartheta)-n(s,\vartheta)Iu(s), \tag{7a}$$

$$\eta\frac{dI}{d\vartheta}=[-1+\overline{n(s,\vartheta)u(s)}]I, \tag{7b}$$

where

$$u(s)=(1-\cos2\pi s) \tag{8}$$

and the overbar denotes an integration over the whole spatial period,

$$\overline{f(s)}\equiv\int_0^1 f(s)ds. \tag{9}$$

Here, we have replaced integral (6) with integral (9) due to the equalities

$$\langle f(x)\rangle=\kappa\sum_{n=0}^{\infty}\int_n^{(n+1)l}e^{-\kappa x}f(x)dx\approx\kappa\sum_{n=0}^{\infty}e^{-\kappa ln}\int_0^l f(x)dx$$

$$\approx\kappa\int_0^\infty e^{-\kappa ly}dy\int_0^l f(x)dx=\frac{1}{l}\int_0^l f(x)dx=\overline{f(s)} \tag{10}$$

that approximately hold for any periodic function $f(x)=f(x+l)$ provided $\kappa l\ll1$. For the given values of the parameters, we have $l\approx2\times10^{-5}$ and $\kappa l\approx2.5\times10^{-4}$.

Denote the steady state solution of Eqs. (7) corresponding to a fixed pump level w_0 by n^0 and I^0 and consider the dynamics of the system in the vicinity of that solution. Substituting

$$w=w_0+\Delta w, \tag{11a}$$

$$n(s,\vartheta)=n^0(s)+\eta\varphi(s,\vartheta) \tag{11b}$$

into Eq. (7), we obtain the equations for the variables φ and I

$$\frac{d}{d\vartheta}\varphi(s,\vartheta)=\Delta w+\frac{w_0(I^0-I)u(s)}{1+I^0u(s)}-\eta[1+Iu(s)]\varphi(s,\vartheta), \tag{12a}$$

$$\frac{dI}{d\vartheta}=\overline{\varphi(s,\vartheta)u(s)}I, \tag{12b}$$

where the steady state values $n^0(s)$ and I^0 in a nonexplicit form are defined by

$$w_0=w_0(I^0)=\left[\overline{\left(\frac{u}{1+I^0u}\right)}\right]^{-1}=\frac{I^0\sqrt{1+2I^0}}{\sqrt{1+2I^0}-1}, \tag{13a}$$

$$n^0(s)=\frac{w_0(I^0)}{1+I^0u(s)}. \tag{13b}$$

To find an approximate solution of the system (12), we introduce the moments of the function $\varphi(s,\vartheta)$. The jth moment we define as

$$G^{(j)}=\overline{\varphi(s,\vartheta)u^j(s)}. \tag{14}$$

To derive equations for the moments, we multiply Eq. (12a) by the function $u^j(s)$ and integrate it over the whole interval of the space variable s:

$$\frac{dG^{(j)}}{d\vartheta}=\Delta w\overline{u^j}+w_0(I^0-I)J_{j+1}-\eta G^{(j)}-\eta IG^{(j+1)},$$

$$j=1,2,\ldots, \tag{15}$$

where the coefficients

$$J_j=\overline{\left(\frac{u^j}{1+I^0u}\right)} \tag{16}$$

can easily be calculated from the iterative relation

$$J_j=(\overline{u^{j-1}}-J_{j-1})/I^0 \tag{17}$$

with the first term equal to

$$J_0=(1+2I^0)^{-1/2}. \tag{18}$$

The integrals $\overline{u^j}$ in Eqs. (15) and (17) can be calculated analytically; the first three values of these integrals are $\overline{u^0}=1$, $\overline{u^1}=1$, and $\overline{u^2}=3/2$.

Equation (15) for the jth moment contains the higher moment $j+1$ and, hence, we have an infinite set of coupled ordinary differential equations that includes all orders of moments. We can, however, truncate this system owing to the smallness of the parameter η. Consider the equations for the first two moments,

$$\frac{dG^{(1)}}{d\vartheta}=\Delta w+w_0J_2(I^0-I)-\eta G^{(1)}-\eta IG^{(2)}, \tag{19a}$$

$$\frac{dG^{(2)}}{d\vartheta}=\frac{3}{2}\Delta w+w_0J_3(I^0-I)-\eta G^{(2)}-\eta IG^{(3)}. \tag{19b}$$

To determine the variation rate of $G^{(1)}$ with accuracy $O(\eta)$, it suffices to find the value of $G^{(2)}$ with accuracy $O(1)$. Thus, the $O(\eta)$ terms in Eq. (19b) are nonessential ones, and we can omit the term containing the third moment $G^{(3)}$. However, we do not omit the term $-\eta G^{(2)}$ to preserve the stability of Eq. (19b). After omitting the moment $G^{(3)}$ in Eq. (19b), the system (19) together with Eq. (12b), which can be presented in the form $dI/d\vartheta=G^{(1)}I$, make up a closed system of ordinary differential equations for the variables $G^{(1)}$, $G^{(2)}$, and I. We can expect that the solution of this system will coincide with the solution of the original space-dependent rate equations (12) with accuracy $O(\eta)$. Before verifying this proposition numerically we simplify Eqs. (19) further. The moment $G^{(2)}$ can be excluded from Eqs. (19) as follows. Expressing variable $w_0(I^0-I)$ from Eq. (19a), substituting it into Eq. (19b), and integrating the resulting equation, we obtain

$$G^{(2)}=\frac{J_3}{J_2}G^{(1)}+\left(\frac{3}{2}-\frac{J_3}{J_2}\right)\int^{\vartheta}\Delta w(\vartheta')d\vartheta'+O(\eta). \tag{20}$$

The integral $P=\int^{\vartheta}\Delta w(\vartheta')d\vartheta'$ in Eq. (20) can be modeled with accuracy $O(1)$ by an additional equation $dP/d\vartheta=\Delta w-\eta P$. Substituting Eq. (20) into Eq. (19a) and collecting other required equations, we end up with the closed system

$$\frac{dI}{d\vartheta}=G^{(1)}I, \tag{21a}$$

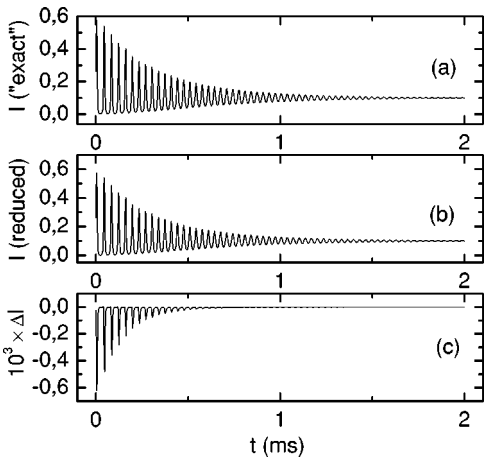

FIG. 1. Comparison of solutions of (a) the initial space-dependent rate equations (12) and (b) the reduced system (22) for the pump rate $w_0=1.14$ and the amplitude of the initial perturbation $A=1$. In (c) is shown the difference between these two solutions. The intensities are shown in arbitrary units.

$$\frac{dG^{(1)}}{d\vartheta}=\Delta w+w_0J_2(I^0-I)-\eta\left(1+\frac{J_3}{J_2}I\right)G^{(1)}-\eta\left(\frac{3}{2}-\frac{J_3}{J_2}\right)IP, \tag{21b}$$

$$\frac{dP}{d\vartheta}=\Delta w-\eta P \tag{21c}$$

that models the dynamics of the original space-dependent rate equations (12) with accuracy $O(\eta)$.

In the case of a small additional pump rate Δw, the system can be simplified even more. The last term on the right-hand side of Eq. (21b) can be omitted, since P is $O(\Delta w)$ and this term is $O(\eta\Delta w)$. Omitting the last term in Eq. (21b) and simplifying the notation $G^{(1)}\equiv G$, we finally get the closed system of two ordinary differential equations:

$$\frac{dI}{d\vartheta}=GI, \tag{22a}$$

$$\frac{dG}{d\vartheta}=\Delta w+w_0J_2(I^0-I)-\eta\left(1+\frac{J_3}{J_2}I\right)G. \tag{22b}$$

To verify the accuracy of Eqs. (22), we analyzed numerically the transient dynamics of the single-mode laser. For the system initially in the steady state at the pump rate w_0, we applied an additional short pulse $\Delta w(t)=A\,\delta(t)$, where $\delta(t)$ is the Dirac delta function, and considered the recurrence dynamics to the initial state. In Fig. 1, we compare the results of the simulation of the original space-dependent rate equations (12) and Eqs. (22) for $w_0=1.14$, $A=1$. To simulate Eqs. (12) we subdivided the fundamental interval of the space variable $s\in[0,1]$ into $M_s=10^3$ equal discrete cells and ascribed them M_s variables $\varphi(s_i,\vartheta)$, $i=1,\ldots,M_s$, where s_i is the value of s associated with the ith cell. The solution was obtained by integrating M_s+1 ordinary differ-

ential equations for the variable I and M_s variables $\varphi(s_i,\vartheta)$. The initial conditions for Eqs. (22) are $G(0)=0$ and $I(0)=I^0$. For Eqs. (12), we have chosen the same initial condition $I(0)=I^0$ and tried various initial distributions $\varphi(s,0)$, satisfying the requirement $\overline{\varphi(s,0)u(s)}=0$ compatible with the condition $G(0)=0$. The result is independent of the details of the initial distribution $\varphi(s,0)$, provided the condition $\overline{\varphi(s,0)u(s)}=0$ is fulfilled.

As expected, the difference between the solutions of Eqs. (12) and Eqs. (22) is $O(\eta)$ [Fig. 1(c)]. Thus, the reduced system of two ordinary differential equations (22) quantitatively models the dynamics of the original space-dependent rate equations (12).

We succeeded with our reduction procedure mainly due to a right choice of the characteristic scales for the variables involved in Eqs. (2). Upon transformation of these equations into the dimensionless form (12), we were able to utilize the smallness of the parameter η. We expanded the solution into moments [see Eq. (14)] and derived for them an infinite set of coupled ordinary differential equations (15). Then these equations were truncated at the small term containing higher moments and a closed system of ordinary differential equations was obtained [see Eq. (22)]. In the next section, we generalize the above reduction procedure for the case of a multimode laser.

B. Multimode laser

For the multimode case, we use the same substitution (11) in Eqs. (3) and obtain a generalized version of Eqs. (12):

$$\frac{d}{d\vartheta}\varphi(x,\vartheta)=\Delta w+\frac{w_0\Sigma_i(I_i^0-I_i)u_i(x)}{1+\Sigma_i I_i^0 u_i(x)}-\eta\left[1+\sum_i I_i u_i(x)\right]\varphi(x,\vartheta), \tag{23a}$$

$$\frac{dI_j}{d\vartheta}=G_j I_j, \tag{23b}$$

where

$$G_j=\langle\varphi(x,\vartheta)u_j(x)\rangle \tag{24}$$

is the first moment of the function $\varphi(x,\vartheta)$ corresponding to the jth mode. The steady state values of the population inversion $n^0(x)$ and the intensities I_i^0, appropriate to a fixed value of the pump rate w_0, satisfy the equalities

$$w_0\left\langle\frac{u_j(x)}{1+\Sigma_i I_i^0 u_i(x)}\right\rangle-1=0, \tag{25a}$$

$$n^0(x)=\frac{w_0}{1+\Sigma_i I_i^0 u_i(x)}. \tag{25b}$$

Equation (25a) defines the only nonvanishing intensities I_i^0. This means that the indices i and j in Eq. (25a) are varied only among the values corresponding to the lasing modes, i.e., the modes whose steady state intensities are not zero. The problem of the mode configuration, i.e., the question of how many and which modes are present at a fixed pump rate w_0, will be discussed below. Now, we suppose that the mode configuration is known and, for the given configuration, obtain the reduced system of rate equations.

To derive the equations for the moments G_j, we multiply Eq. (23a) by the function $\kappa e^{-\kappa x}u_j(x)$ and integrate it over the space variable x:

$$\frac{dG_j}{d\vartheta}=\Delta w\langle u_j(x)\rangle+w_0\sum_i\beta_{ij}(I_i^0-I_i)-\eta G_j-\eta\sum_i M_{ij}I_i. \tag{26}$$

Here the coefficients β_{ij} are

$$\beta_{ij}=\left\langle\frac{u_i(x)u_j(x)}{1+\Sigma_m I_m^0 u_m(x)}\right\rangle \tag{27}$$

and

$$M_{ij}=\langle\varphi(x,\vartheta)u_i(x)u_j(x)\rangle \tag{28}$$

is the matrix element corresponding to the second-order moments of the unknown function $\varphi(x,\vartheta)$. Note that the matrices β and M are both symmetric, $\beta_{ij}=\beta_{ji}$ and $M_{ij}=M_{ji}$. Equation (26) relates the first-order moment G_j to the second-order moments M_{ij}. However, the contribution of the second-order moments in this equation is small, since the corresponding terms are proportional to η. Hereafter, we suppose that the parameter Δw is also small. To determine the variation rate of the first-order moments $dG_j/d\vartheta$ with accuracy $O(\eta,\Delta w)$, it suffices to estimate the second-order moments M_{ij} with accuracy $O(1)$. The equations for the second-order moments M_{ij} are obtained from Eq. (23a) by multiplying it by the function $\kappa e^{-\kappa x}u_i(x)u_j(x)$ and integrating over the space variable x:

$$\frac{dM_{ij}}{d\vartheta}=w_0\sum_k\gamma_{ijk}(I_k^0-I_k), \tag{29}$$

where

$$\gamma_{ijk}=\left\langle\frac{u_i(x)u_j(x)u_k(x)}{1+\Sigma_m I_m^0 u_m(x)}\right\rangle. \tag{30}$$

Here, we omitted the terms that are proportional to η and Δw. Equation (29) for the second-order moments can be

solved analytically. To do this, we solve Eq. (26) with respect to the variables $w_0(I_i^0-I_i)$. With accuracy $O(1)$, we obtain

$$w_0(I_i^0-I_i)=\sum_k (\beta^{-1})_{ij}\frac{dG_j}{d\vartheta}, \tag{31}$$

where β^{-1} is the inverse of the matrix β. Substituting Eq. (31) into Eq. (29) and integrating with respect to time ϑ, we find the following relationship between the second- and first-order moments:

$$M_{ij}=\sum_j T_{ijk}G_k, \tag{32}$$

where

$$T_{ijk}=\sum_m \gamma_{mij}(\beta^{-1})_{mk}. \tag{33}$$

The relationship (32) is valid with accuracy $O(1)$. From Eqs. (23b), (26), and (32), we finally obtain the closed system

$$\frac{dI_j}{d\vartheta}=G_jI_j, \tag{34a}$$

$$\frac{dG_j}{d\vartheta}=\Delta w\langle u_j(x)\rangle+w_0\sum_i \beta_{ij}(I_i^0-I_i)-\eta G_j$$

$$-\eta\sum_{im} T_{ijm}I_iG_m \tag{34b}$$

that represents the generalized version of Eqs. (22) for the multimode case. The indices *i*, *j*, and *m* in Eqs. (34) are varied only among the lasing modes whose steady state intensities are not zero. Thus, in the case of *N* lasing modes, the space-dependent rate equations (23) can be reduced to the system (34) of $2N$ ordinary differential equations.

1. Steady state solution

The steady state intensities I_i^0 of the lasing modes satisfy Eq. (25a). To find out which modes are really present at a fixed value of the pump rate w_0, we have to analyze the steady state solutions of the system (3) at $w=w_0$ in more detail. All steady state solutions of this system are defined by the equation $G_j^0I_j^0=0$, where

$$G_j^0=w_0\left\langle\frac{u_j(x)}{1+\Sigma_iI_i^0u_i(x)}\right\rangle-1 \tag{35}$$

is the steady state value of the expression in angular brackets that appears in Eq. (3b). The equation $G_j^0I_j^0=0$ can be satisfied by setting either $G_j^0=0$ or $I_j^0=0$. The stable mode configurations must satisfy (I) $G_j^0=0$, if $I_j^0\neq 0$ and (II) $G_j^0<0$, if $I_j^0=0$. The first condition is equivalent to Eq. (25a) and defines the intensities of the lasing (nonvanishing) modes. The second condition guarantees the stability of the given mode configuration with respect to all vanishing modes, i.e., the modes whose steady state intensities are zero. This conclusion follows from the linearized Eq. (3b). The small intensity fluctuations δI_j of the vanishing modes $I_j^0=0$, $G_j^0\neq 0$ are governed by the equation $\eta d\,\delta I_j/d\vartheta=G_j^0\,\delta I_j$. Thus, G_j^0 has the simple physical meaning that it defines the increment of the *j*th vanishing mode. Condition (II) guarantees that the increments of all vanishing modes are negative and, hence, small fluctuations related to these modes decay.

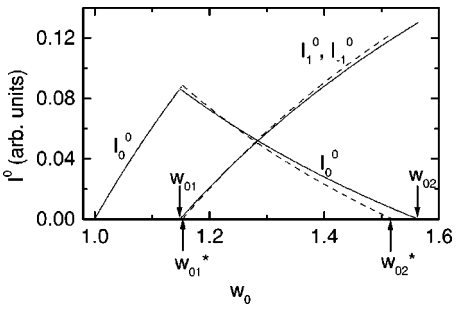

FIG. 2. Dependence of the steady state intensities on the pump rate w_0. The dashed lines show almost the same dependence in the presence of an intracavity frequency doubling KTP crystal.

An analytical solution of Eq. (25a) is generally not available. However, we can find an approximate solution provided that the pump rate w_0 is not too much above the threshold value. Following Ref. [11], we suppose that the intensities I_i^0 are small and use an approximation

$$\frac{1}{1+\Sigma_iI_i^0u_i(x)}\approx 1-\sum_i I_i^0u_i(x) \tag{36}$$

that transforms Eq. (25a) into a linear system. To find an explicit solution of this system, we have to calculate the following integrals:

$$\langle u_i\rangle\approx g_i, \tag{37a}$$

$$\langle u_iu_j\rangle\approx g_ig_j(1+K_{i-j}/2), \tag{37b}$$

where

$$K_m\equiv\langle\cos(2\pi mx)\rangle=(1+\zeta m^2)^{-1},\quad \zeta=(2\pi/\kappa)^2. \tag{38}$$

In Eqs. (37), we omitted small terms that are proportional to $1/\zeta M^2\approx 1.6\times 10^{-9}$, where *M* is the number of half wavelengths along the laser cavity. From Eqs. (35), (36), and (37), we obtain

$$G_j^0=g_jw_0\left[1-\sum_i\left(1+\frac{K_{i-j}}{2}\right)g_iI_i^0\right]-1. \tag{39}$$

Now, we are ready to investigate the dependence of the steady state solution on the pump rate w_0. The numerical illustration of this dependence is presented in Fig. 2. We start

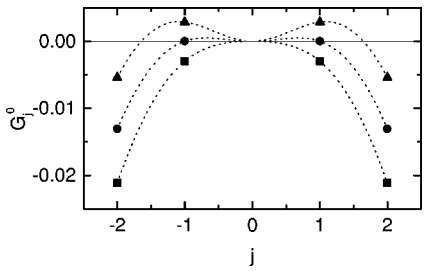

FIG. 3. Increments G_j^0 $(j=\pm1,\pm2)$ of the vanishing modes for the single-mode laser. The values G_j^0 are calculated from Eq. (41) at various values of the pump rate w_0. The full squares, circles, and triangles correspond to $w_0=1.1<w_{01}$, $w_0=w_{01}\approx1.149$, and $w_0=1.2>w_{01}$, respectively.

with small values of w_0 when there exists only a single lasing mode, $I_0^0\neq0$ and $I_i^0=0$ for $i=\pm1,\pm2,\ldots$. From the condition $G_0^0=0$, we have

$$I_0^0=\frac{2}{3}\left(1-\frac{1}{w_0}\right). \tag{40}$$

The intensity I_0^0 is positive at $w_0>1$. This means that the first laser threshold is $w_0=1$. The increments of the vanishing modes are

$$G_j^0=g_jw_0\left[1-\left(1+\frac{K_j}{2}\right)\frac{2}{3}\left(1-\frac{1}{w_0}\right)\right]-1, \quad j=\pm1,\pm2,\ldots. \tag{41}$$

These increments are presented in Fig. 3 for various values of the pump rate w_0. They are negative, $G_j^0<0$, $j=\pm1$, $\pm2,\ldots$, when $w_0<w_{01}$, where

$$w_{01}=1+3\xi(1+1/\zeta) \tag{42}$$

is the threshold of three-mode operation. The value w_{01} is defined by the condition $G_1^0=G_{-1}^0=0$. Just above the threshold $w_0>w_{01}$, the increments G_1^0 and G_{-1}^0 become positive. This means that the single-mode configuration becomes unstable with respect to two symmetrical neighboring modes that are labeled with the subscripts $i=\pm1$. Thus, for $w_0>w_{01}$, we have to take into account three modes when calculating the sum in Eq. (39).

For the three-mode configuration $I_0^0\neq0$, $I_1^0=I_{-1}^0\neq0$, and $I_i^0=0$, $i=\pm2,\pm3,\ldots$, the intensities I_0^0 and $I_{\pm1}^0$ are obtained from the conditions $G_0^0=0$, $G_{\pm1}^0=0$, which yield a system of two linear equations with respect to I_0^0 and I_1^0. Upon solving this system, we obtain

$$I_0^0=2\frac{(w_0-1)(1-2K_1+K_2)+2\xi(2+K_1)}{w_0(7-8K_1-2K_1^2+3K_2)}, \tag{43a}$$

$$I_1^0=I_{-1}^0=2\frac{(w_0-1)(1-K_1)-3\xi}{g_1w_0(7-8K_1-2K_1^2+3K_2)}. \tag{43b}$$

The intensity I_1^0 is equal to zero at $w_0=w_{01}$ and is positive when $w_0>w_{01}$. Thus, the condition $I_1^0=0$ gives an alternative possibility for determining the threshold of the three-mode configuration. Above the threshold w_{01}, the intensities I_1^0 and I_{-1}^0 increase with increasing w_0, while the intensity I_0^0 decreases and turns to zero at $w_0=w_{02}$, where

$$w_{02}=w_{01}+\xi\frac{17+14\zeta}{1-2\zeta}. \tag{44}$$

Inside the interval $w_{01}<w_0<w_{02}$, the vanishing modes have negative increments, $G_j^0<0$ for $j=\pm2,\pm3,\ldots$. Thus, the three-mode configuration (43) is stable with respect to the vanishing modes in the whole interval $w_{01}<w_0<w_{02}$. For given values of the parameters, the boundaries of the interval are $w_{01}\approx1.149$ and $w_{02}\approx1.564$.

In a similar manner, the steady state solution can be continued in the region $w_0>w_{02}$; however, we cannot go to much above the laser threshold, since we used approximation (36). In the subsequent discussion, we restrict ourselves to values $w_0<w_{02}$ and analyze the transient response of a three-mode laser excited by a short pulse of the pump rate.

2. Transient dynamics

The dynamics of the system close to the steady state, defined by a fixed pump rate w_0, is described by Eqs. (34). To solve Eqs. (34) we need to know the coefficients β_{ij} and T_{ijk}. The latter is related to the coefficients γ_{ijk} by Eq. (33). We exploited the already used approximation (36) in order to estimate these coefficients. From Eqs. (27) and (30), we obtain

$$\beta_{ij}\approx\langle u_i(x)u_j(x)\rangle-\sum_m I_m^0\langle u_m(x)u_i(x)u_j(x)\rangle, \tag{45}$$

$$\gamma_{ijk}\approx\langle u_i(x)u_j(x)u_k(x)\rangle-\sum_m I_m^0\langle u_m(x)u_i(x)u_j(x)u_k(x)\rangle. \tag{46}$$

We have already calculated the integral $\langle u_iu_j\rangle$ in Eq. (37b). Similarly, one can calculate the integrals involving the products of three and four u functions:

$$\langle u_iu_ju_k\rangle\approx g_ig_jg_k[1+(K_{i-j}+K_{i-k}+K_{j-k})/2], \tag{47}$$

$$\langle u_iu_ju_ku_m\rangle\approx g_ig_jg_kg_m[1+(K_{i-j}+K_{i-k}+K_{i-m}+K_{j-k}+K_{j-m}+K_{k-m})/2+(K_{i+j-k-m}+K_{i-j-k+m}+K_{i-j+k-m})/8], \tag{48}$$

where K_m is defined in Eq. (38). Here, as well as in Eqs. (37), we omitted small terms that are proportional to $1/\zeta M^2$.

In Fig. 4, we present the transient behavior of the three-mode laser excited from a steady state by a short pulse of the pump rate $\Delta w=A\delta(t)$ with $A=1$. The pump rate $w_0=1.25$ is chosen inside the interval $[w_{01},w_{02}]$ so that Eqs. (43) are valid for the steady state intensities I_0^0 and $I_{-1}^0=I_1^0$. Equations (34) were integrated with the initial conditions $I_0(0)=I_0^0$, $I_{-1}(0)=I_1^0(0)=I_1^0$, and $G_0(0)=G_1(0)=G_{-1}(0)=0$. It is seen from Fig. 4 that the total intensity

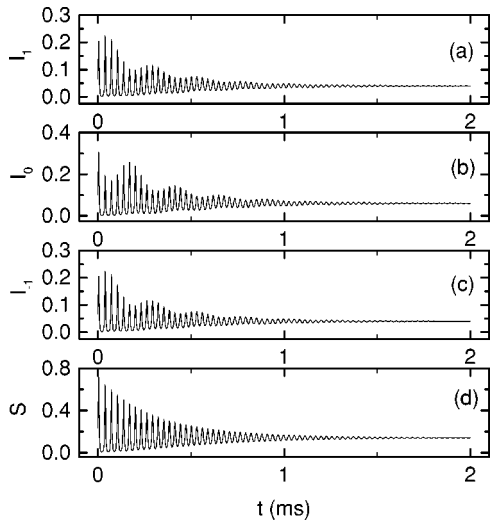

FIG. 4. Transient behavior of the intensities (in arbitrary units) of the three-mode laser excited by a short pulse of the pump rate for $w_0=1.25$ and $A=1$. (a),(b),(c) give the dynamics of the partial intensities of different modes and (d) that of the total intensity $S=I_0+I_1+I_{-1}$.

displays a much smoother behavior than each partial intensity. The total intensity relaxes to its steady state with a single characteristic frequency, while the partial intensities have more characteristic frequencies. This effect is known as antiphase dynamics and is typical for multimode Fabry-Pérot lasers [13].

IV. DYNAMICS OF A FREQUENCY DOUBLED LASER

In this section, we derive the dynamical equations of a multimode laser in the presence of an intracavity frequency doubling crystal, made from KTP. The KTP crystal causes a nonlinear frequency conversion that has to be incorporated in Eq. (3b) as a loss term for the infrared light. Following Ref. [6], we take into account the birefringence of optical elements in the cavity and the harmonic conversion efficiency of the fundamental intensity. Then, Eq. (3b) which describes the variation rate of the intensity of the jth mode transforms to

$$\eta\frac{dI_j}{d\vartheta}=\left[-1+\langle n(x,\vartheta)u_j(x)\rangle-\frac{\epsilon}{\alpha}\left(gI_j+2\sum_{i\neq j}\mu_{ij}I_i\right)\right]I_j. \tag{49}$$

Here, g is a geometrical factor whose value depends on the optical phase delay through the amplifying and the doubling crystals and on the angle between their fast axes. Both the Nd:YAG crystal and the KTP crystal are birefringent. The birefringence leads to two orthogonal directions of polarization as eigenstates of the cavity. Moreover, we have $\mu_{ij}=g$ if modes i and j have the same polarization, while $\mu_{ij}=1-g$ if these modes are orthogonally polarized. ϵ is a nonlinear coefficient whose value depends on the properties of the KTP crystal. The values of the parameters g and ϵ used in our numerical analysis are presented in Table I.

The system of space-dependent rate equations (3a) and (49), defining the dynamics of an intracavity frequency doubled laser, can be reduced, following the same scheme as described in Sec. III B. Using substitution (11) for the function $\varphi(x,\vartheta)$, we obtain the same equation (23a) as in the case without the KTP crystal, while Eq. (23b)—for intensities—changes to the form

$$\frac{dI_j}{d\vartheta}=\left\{G_j-\frac{\epsilon}{\alpha\eta}\left[g(I_j-I_j^0)+2\sum_{i\neq j}\mu_{ij}(I_i-I_i^0)\right]\right\}I_j. \tag{50}$$

The steady state intensities corresponding to a fixed value of the pump rate w_0 are now defined by the equations

$$w_0\left\langle\frac{u_j(x)}{1+\Sigma_i I_i^0u_i(x)}\right\rangle-1-\frac{\epsilon}{\alpha}\left(gI_j^0+2\sum_{i\neq j}\mu_{ij}I_i^0\right)=0. \tag{51}$$

In the presence of the KTP crystal, Eq. (23a) remains unchanged and the reduction procedure described in Sec. III B can be exactly repeated in that case. As a result, we obtain the same Eq. (34b) as in the case without the KTP crystal for the moments G_j:

$$\frac{dG_j}{d\vartheta}=\Delta w\langle u_j(x)\rangle+w_0\sum_i\beta_{ij}(I_i^0-I_i)$$
$$-\eta G_j-\eta\sum_{im}T_{ijm}I_iG_m. \tag{52}$$

Equations (50) and (52) form a closed system of ordinary differential equations that describe the dynamics of an intracavity frequency doubled multimode laser close to the steady state defined by Eq. (51).

In order to numerically analyze the possible influence of the KTP crystal on the steady state and the dynamical properties of the laser, we again employ approximation (36). Then Eq. (51) for the steady state intensities I_j^0 transforms to

$$g_jw_0\left[1-\sum_i\left(1+\frac{K_{i-j}}{2}\right)g_iI_i^0\right]-1-\frac{\epsilon}{\alpha}\left(gI_j^0+2\sum_{i\neq j}\mu_{ij}I_i^0\right)=0. \tag{53}$$

For the single-mode laser $I_0^0\neq0$ and $I_j^0=0$, $j=\pm1,\pm2,\ldots$, we obtain

$$I_0^0=\frac{w_0-1}{3w_0/2+\epsilon g/\alpha}. \tag{54}$$

Without the KTP crystal, we have $\epsilon=0$; this equation coincides with Eq. (40).

In the case of three-mode operation $I_0^0\neq0$, $I_{\pm1}^0$ and $I_j^0=0$, $j=\pm2,\pm3,\ldots$, Eqs. (53) transform to a system of two linear equations

$$\left[\frac{3}{2}+\frac{\epsilon g}{\alpha w_0}\right]I_0^0+\left[(2+K_1)g_1+\frac{4\epsilon(1-g)}{\alpha w_0}\right]I_1^0=1-\frac{1}{w_0}, \tag{55a}$$

$$\left[1+\frac{K_1}{2}+\frac{2\epsilon(1-g)}{\alpha w_0 g_1}\right]I_0^0+\left[\left(2+\frac{1+K_2}{2}\right)g_1+\frac{3\epsilon g}{\alpha w_0 g_1}\right]I_1^0 =1-\frac{1}{w_0 g_1} \tag{55b}$$

that define the intensities I_0^0 and I_1^0. The intensity I_{-1}^0 satisfies the equality $I_{-1}^0=I_1^0$. Here and below, we suppose that the modes I_1^0 and I_{-1}^0 have the same direction of polarization, while the modes I_0^0 and $I_{\pm 1}^0$ have orthogonal directions of polarizations, i.e., we take $\mu_{0,0}=\mu_{-1,1}=g$ and $\mu_{0,1}=\mu_{0,-1}=1-g$. In the case $\epsilon=0$, the solution is defined by Eqs. (43). Figure 2 illustrates how the KTP influences this solution. The dotted lines correspond to the case when the KTP crystal is taken into account. The dependencies of the steady state intensities on w_0 are calculated from Eqs. (54) and (55) at $\epsilon=2\times10^{-5}$. As is seen from the figure, the KTP crystal only slightly influences the steady state solution. This is because the terms responsible for frequency doubling in Eqs. (54) and (55) are relatively small; they are proportional to $\epsilon/\alpha=0.002$. The KTP crystal also slightly changes the thresholds w_{01} and w_{02} that define the boundaries of the three-mode operation. We mark the corresponding thresholds determined with the KTP crystal by stars; they are approximately $w_{01}^*\approx1.153$ and $w_{02}^*\approx1.519$.

Although the KTP crystal only slightly influences the steady state solution, it essentially changes the dynamical properties of the system. The nonlinear conversion can cause an instability of the steady state. As a result, the output intensities can exhibit periodic or chaotic oscillations around the unstable steady state. These oscillations exist at a fixed value of the pump rate, $w_0=\text{const}$ and $\Delta w=0$. An example of the chaotic oscillations that the system exhibits in the three-mode operation at $w_0=1.25$ is presented in Fig. 5. The results were obtained via numerical integration of Eqs. (50) and (52). Here as well as in Fig. 4 a pronounced antiphase dynamics is observed. Note that a chaotic antiphase dynamics was first reported and analyzed in the framework of the JHBWR model in Ref. [5].

One part of the reason why the KTP crystal affects the dynamical properties much more than the steady state is that the terms responsible for frequency doubling have different weights in Eqs. (50) and (51). In Eq. (50), defining the dynamics of the intensities, these terms are proportional to $\epsilon/\alpha\eta\approx0.287$ and are $1/\eta$ times larger than the corresponding terms in Eq. (51), defining the steady state solution.

In order to gain a better insight into the instability caused by the KTP crystal, we performed a linear analysis of Eqs. (50) and (52). The dynamics of the small deviations $\delta I_j=I_j-I_j^0$, $\delta G_j=G_j$ from the steady state is described by a linearized system of Eqs. (50) and (52):

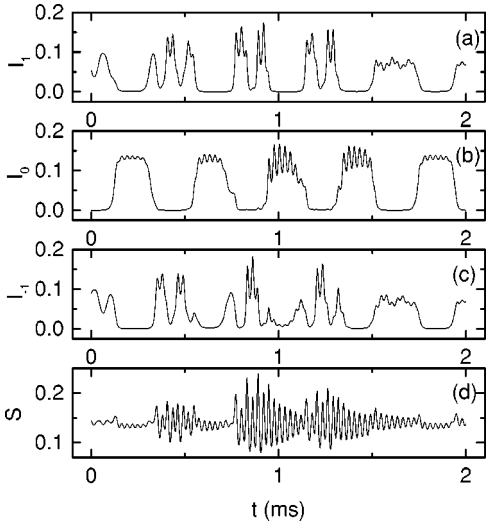

FIG. 5. Chaotic oscillations of the intensities (in arbitrary units) of the three-mode laser with the KTP crystal at a fixed value of the pump rate, $w_0=1.25$. (a),(b),(c) give the dynamics of the partial intensities of different modes and (d) that of the total intensity $S=I_0+I_1+I_{-1}$.

$$\frac{\delta I_j}{d\vartheta}=\left\{\delta G_j-\frac{\epsilon}{\alpha\eta}\left[g\,\delta I_j+2\sum_{i\neq j}\mu_{ij}\delta I_i\right]\right\}I_j^0, \tag{56a}$$

$$\frac{d\,\delta G_j}{d\vartheta}=\Delta w\langle u_j\rangle-w_0\sum_i\beta_{ij}\delta I_i-\eta\delta G_j-\eta\sum_{im}T_{ijm}I_i^0\,\delta G_m. \tag{56b}$$

For $\Delta w=0$, this system can be solved by an exponential substitution $\delta I_j\propto\exp(\lambda\vartheta)$ and $\delta G_j\propto\exp(\lambda\vartheta)$, where λ defines the eigenvalues of the system. The eigenvalues λ satisfy a characteristic equation that in the case of N lasing modes represents a $2N$-order polynomial. The steady state is stable if the real parts of all roots of the characteristic polynomial are negative, $\mathrm{Re}\,\lambda_j<0$, $j=1,2,\ldots,2N$.

The results of a linear stability analysis for the three-mode operation are presented in Fig. 6. Here, the maximum real part of the eigenvalues is plotted versus the pump rate w_0. As

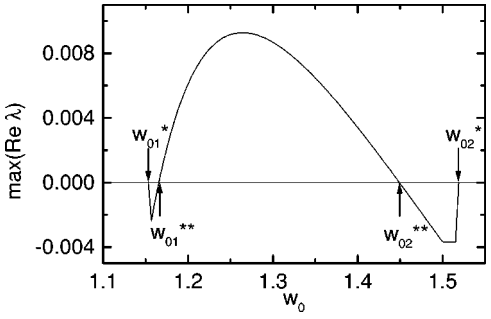

FIG. 6. The maximum real part of the eigenvalues of the linearized Eq. (56) versus the pump rate w_0. The values w_{01}^* and w_{02}^* define the boundaries of the three-mode operation, the values w_{01}^{**} and w_{02}^{**} the thresholds of instability.

is clearly seen from the figure, the three-mode configuration is stable only in small intervals $w_{01}^{*}<w_0<w_{01}^{**}$ and $w_{02}^{**}<w_0<w_{02}^{*}$ close to the thresholds w_{01}^{*} and w_{02}^{*} defining the boundaries of this configuration. The interval $w_{01}^{**}<w_0<w_{02}^{**}$, corresponding to the unstable steady state solution is relatively large. The thresholds of the instability are approximately $w_{01}^{**}\approx 1.167$ and $w_{02}^{**}\approx 1.445$.

Note that, without the KTP crystal ($\epsilon=0$), the three-mode configuration is stable in the whole interval $w_{01}<w_0<w_{02}$. Numerical analysis shows that the two last terms in Eq. (56b) which are proportional to η provide the stability of the steady state. Without these terms ($\eta=0$), all eigenvalues are purely imaginary and small deviations from the steady state exhibit undamped oscillations. The terms that are proportional to η cause a small damping. Due to these terms, the eigenvalues gain small negative real parts proportional to η, and the system approaches the steady state by slow relaxation oscillations (Fig. 4). When the KTP crystal is taken into account ($\epsilon\neq 0$), the last two terms in Eq. (56a) that are proportional to $\epsilon/\alpha\eta$ work in an opposite manner, i.e., they destabilize the steady state. Thus, the result depends on the concurrence between the small terms in Eq. (56b) that are proportional to η and those in Eq. (56a) that are proportional to $\epsilon/\alpha\eta$. Because the stability problem is sensitive to small terms it is evident that the procedure of reducing the spatial degrees of freedom requires a high accuracy. In our approach, we thoroughly performed this reduction taking into account all terms down to and including $O(\eta)$.

V. STABILIZING THE STEADY STATE

In our previous work [8], we considered the problem of stabilizing the steady state of the multimode laser in the framework of the JHBWR model. We modulated the pump rate of the laser by a feedback signal composed of two total output intensities of infrared light polarized in two different orthogonal directions. Analyzing various control techniques, we came to the conclusion that the most appropriate for experimental application is the proportional feedback technique. Here, we apply this technique to our reduced system of Eqs. (50) and (52). For the three-mode operation, the proportional feedback is defined by the equation

$$\Delta w = k_x \delta I_0 + k_y(\delta I_{-1} + \delta I_1), \tag{57}$$

where $\delta I_j = I_j - I_j^0$ is the deviation of the intensity of the jth mode from its steady state value and k_x, k_y are the feedback amplification coefficients. Recall that, in accordance with our assumption, the modes $j=1$ and $j=-1$ have the same polarization, while the modes $j=0$ and $j=\pm 1$ have orthogonal polarizations. The feedback (57) does not change the steady state solution of Eqs. (50) and (52); however, it can change its stability.

First, we analyze the linear stability of the system under the feedback signal (57). We substitute Eq. (57) into the linearized system (56) and calculate the dependence of its eigenvalues on the feedback parameters k_x and k_y. The main goal is to find the stability domain in the (k_x, k_y) plane that corresponds to the negative real parts of all eigenvalues of the system under feedback control. The results of this analysis are presented in Figs. 7 and 8.

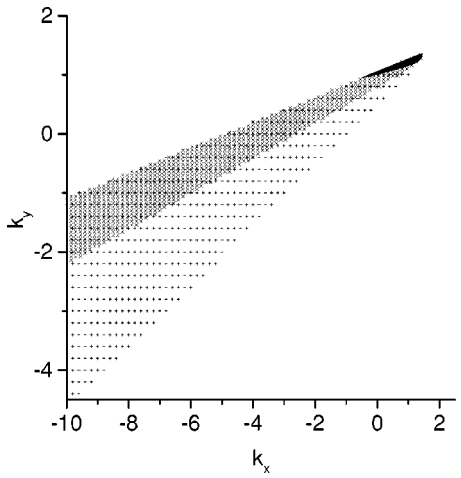

FIG. 7. The domains of stability in the (k_x, k_y) parameter plane for proportional feedback control at different values of the pump rate w_0 (1.168, 1.170, 1.172) taken close to the first threshold of the instability w_{01}^{**}. The darker regions correspond to the larger values of w_0.

Figure 7 illustrates the domains of stability for the pump rate w_0 close to the first threshold w_{01}^{**} of the instability of the three-mode configuration. The darker regions correspond to the large values of the pump rate w_0. As is seen from the figure, the domain of stability decreases with increasing w_0 and disappears at $w_0\approx 1.173$.

In Fig. 8, we start from a pump rate w_0 close to the second threshold w_{02}^{**} of the instability of the three-mode configuration and analyze how the domain of stability in the (k_x, k_y) plane varies on decreasing the pump rate w_0. Here, the darker regions correspond to the smaller values of the pump rate w_0. Again, the domain of stability decreases when

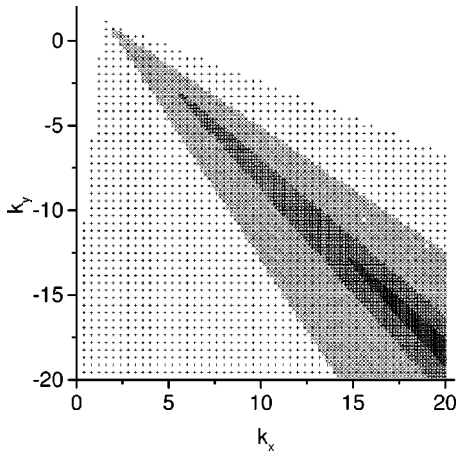

FIG. 8. The same as in Fig. 7, but the values of w_0 (1.400,1.300,1.250,1.245) are started close to the second threshold of the instability w_{02}^{**}. The darker regions correspond to the smaller values of w_0.

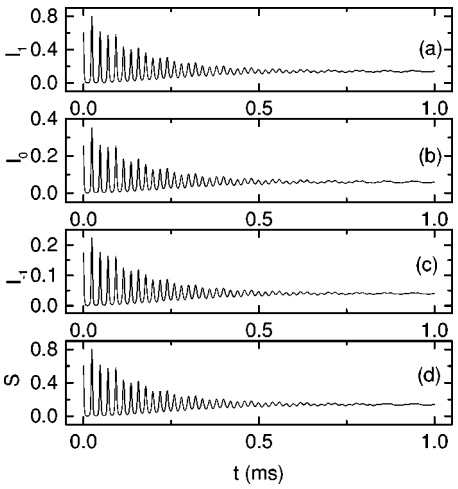

FIG. 9. Transient behavior of the intensities (in arbitrary units) of the three-mode laser with the KTP crystal under proportional feedback control for $w_0=1.25$ and $(k_x,k_y)=(10,-7.5)$. (a),(b),(c) give the dynamics of the partial intensities of different modes and (d) that of the total intensity $S=I_0+I_1+I_{-1}$.

w_0 moves away from the threshold w_{02}^{**} and disappears at $w_0\approx 1.24$. Thus, the three-mode configuration is uncontrollable with proportional feedback in the interval of the pump rate $1.173<w_0<1.24$.

We have verified the results of the linear analysis by integrating the system of nonlinear differential equations (50) and (52). The numerical analysis shows that the linear theory correctly predicts the location of the stability domains. Figure 9 illustrates an example of the system dynamics under proportional feedback control for $w_0=1.25$ and $(k_x,k_y)=(10,-7.5)$. Note that, for the given value w_0, the uncontrolled system exhibits chaotic oscillations, as shown in Fig. 5. Under the feedback signal, the system approaches an initially unstable steady state. The control is successful only when the initial conditions of the system are not too far from the steady state. This means that the stabilized steady state solution has only a finite domain of attraction in phase space. The problem associated with the finite domain of attraction can be overcome by the tracking procedure that we discussed in Ref. [8].

The application of proportional feedback control to the reduced system of Eqs. (50) and (52) leads to results that are somewhat different from those obtained with the JHBWR model [8]. The qualitative difference is that the JHBWR model can be stabilized by proportional feedback for an arbitrarily large pump rate, whereas here, even in the area of relatively small values of the pump rate, we reveal some interval where the system is uncontrollable. On the other hand, the domains of stability presented in Fig. 8 are surprisingly similar to the domains derived from the JHBWR model, although the reduced system of Eqs. (50),(52) and the equations of the JHBWR model differ considerably. In both cases, the domains are bounded by two lines, located in the region of positive values of k_x and negative values of k_y. However, for the JHBWR model, the angle between the lines remains finite at any value of the pump rate w_0, while here these lines merge together at some finite value w_0 and the domain of stability disappears. In general, one can conclude that stabilization of the steady state in our model as well as in a real experiment [9] is much more difficult to achieve than appears from the JHBWR model.

VI. CONCLUSIONS

In summary, we have proposed a quantitatively accurate procedure of reducing the spatial degrees of freedom in a model of space-dependent multimode laser rate equations describing the dynamics of the mode intensities and the population inversion of the active medium. This reduction involves a small parameter that defines the ratio between the population inversion decay rate and the cavity decay rate, which has also been used for spatially nonresolved laser equations by Oppo *et al.* in [14–17]. Unlike the usual consideration, our model incorporates the effects of nonhomogeneous pumping of the active medium. On the basis of the reduced equations, we have numerically analyzed the transient dynamics of the system. For the case of a single-mode operation, we have demonstrated that the solutions of the reduced system are in good quantitative agreement with the solutions of the initial space-dependent rate equations.

We have generalized the reduction procedure for the case of an intracavity frequency doubled Nd:YAG laser. Here, the nonlinear frequency conversion performed by a KTP crystal placed inside the laser cavity was taken into account. Our numerical analysis of the reduced system in this case has shown that the steady state solution may lose its stability and chaotic oscillations of the intensities of different modes may appear. The eigenvalues of the linearized system have real parts that are small compared to the imaginary parts and, thus, the stability of the steady state depends on small parameters. It follows that the procedure of reducing the spatial degrees of freedom requires a high accuracy, in order to correctly predict the stability of the steady state. That is why we have primarily emphasized an accurate derivation of the reduced system.

On the basis of the reduced system, we have reconsidered the problem of controlling the steady state. Previously, we analyzed this problem in the context of the JHBWR model [8]. Here, as well as in Ref. [8], we have shown that the unstable steady state of the system can be stabilized by a proportional feedback control technique, using the laser pump rate as the control parameter and the linear combination of the sum intensities of the infrared laser modes polarized in two different orthogonal directions as the feedback signal. Comparing the results obtained from our reduced system with those obtained from the JHBWR model, one can conclude that our system is less controllable. From the JHBWR model, it follows that the steady state can be stabilized for an arbitrarily large value of the pump rate, whereas our model gives more complex and less optimistic results indicating that it may be uncontrollable even in the area of relatively small values of the pump rate.

Note that the reduced system of Eqs. (50) and (52) is valid for any value of the pump rate. However, in our numerical analysis, we have used approximation (36), which holds only for values that are not too much above the laser threshold.

This represents the only essential approximation that restricts the application area of our numerical analysis. Abandonment of approximation (36), in principle, makes possible the consideration of large values of the pump rate, but it considerably complicates the numerical analysis.

After this work was completed we discovered the recent paper of Mandel [18] where similar ideas were used to analyze the space-dependent laser rate equations.

ACKNOWLEDGMENTS

The authors would like to thank U. Dreßler, A. Schenck zu Schweinsberg, and H. Kantz for fruitful collaboration and discussions. The present work was supported financially by the Max-Planck-Gesellschaft and the Bundesministerium für Bildung, Wissenschaft, Forschung und Technologie (BMBF) under Contract No. 13N7036.

[1] J. Baer, J. Opt. Soc. Am. B **3**, 1175 (1986).
[2] P. Mandel and X.-G. Wu, J. Opt. Soc. Am. B **3**, 940 (1986); X.-G. Wu and P. Mandel, *ibid.* **4**, 1870 (1987).
[3] M. Oka and S. Kubota, Opt. Lett. **13**, 805 (1988).
[4] G.E. James, E.M. Harrel II, C. Bracikowski, K. Wiesenfeld, and R. Roy, Opt. Lett. **15**, 1141 (1990).
[5] C. Bracikowski and R. Roy, Chaos **1**, 49 (1991).
[6] R. Roy, C. Bracikowski, and G.E. James, in *Recent Developments in Quantum Optics*, edited by R. Inguva (Plenum Press, New York, 1993), p. 309.
[7] C. Liu, R. Roy, H.D.I. Abarbanel, Z. Gills, and K. Nunes, Phys. Rev. E **55**, 6483 (1997).
[8] K. Pyragas, F. Lange, T. Letz, J. Parisi, and A. Kittel, Phys. Rev. E **61**, 3721 (2000).
[9] F. Lange, T. Letz, K. Pyragas, J. Parisi, and A. Kittel (unpublished).
[10] A. Schenck and U. Dressler (private communication).
[11] C.L. Tang, H. Statz, and G. deMars, J. Appl. Phys. **36**, 2289 (1963).
[12] E.A. Viktorov, D.R. Klemer, and M.A. Karin, Opt. Commun. **113**, 441 (1995).
[13] P. Mandel, M. Georgeou, K. Otsuka, and D. Pieroux, Opt. Commun. **100**, 341 (1993).
[14] G. Oppo and A. Politi, Z. Phys. B: Condens. Matter **59**, 111 (1985).
[15] G. Oppo and A. Politi, Phys. Rev. A **40**, 1422 (1989).
[16] G. D'Alessandro, A.J. Kent, and G.-L. Oppo, Opt. Commun. **131**, 172 (1996).
[17] D. Henderson and G. Oppo, Phys. Rev. E **59**, 1683 (1999).
[18] P. Mandel, Eur. Phys. J. D **8**, 431 (2000).